ORIGINAL PAPER

Stability in the Kuramoto–Sakaguchi model for finite networks of identical oscillators

Antonio Mihara · Rene O. Medrano-T

Abstract We study the Kuramoto–Sakaguchi model composed by N identical phase oscillators symmetrically coupled. Ranging from local (one-to-one, $R = 1$) to global (all-to-all, $R = N/2$) couplings, we derive a general solution that describes the network dynamics close to an equilibrium. Therewith, we build stability diagrams according to N and R bringing to the light a rich scenery of attractors, repellers, saddles, and non-hyperbolic equilibriums. Our result also uncovers the obscure repulsive regime of the model through bifurcation analysis. Numerical simulations show great accordance with our analytical studies. The exact knowledge of the behavior close to equilibriums may be a fundamental step to investigate phenomena about synchronization in networks. As an example, in the end, we discuss the dynamics behind chimera states from our results.

Keywords Synchronization · Stability · Kuramoto model · Perturbation analysis · Bifurcations

1 Introduction

For more than forty years, the paradigmatic system of N one-dimensional coupled phase oscillators, the

A. Mihara (✉) · R. O. Medrano-T
Depto. de Física, Universidade Federal de São Paulo -
Campus Diadema, Diadema, SP 09913-030, Brazil
e-mail: mihara74@gmail.com

R.O. Medrano-T
e-mail: rmedrano@if.usp.br

Kuramoto model [1], has been intensively studied to understand phenomena related to synchronization in biological, chemical, and electronic networks. Despite the simplicity of the dynamics of each oscillator ($\dot{\theta} = \omega$), strong efforts should be dedicated to find analytical solutions for a network of nonlinearly coupled oscillators, due to the high dimensionality of the system. Kuramoto showed a seminal solution giving rise to the prosper application of the mean–field theory in the Kuramoto model [2]. The method considers the network in the thermodynamic limit $N \to \infty$ with oscillators globally coupled. So that, the network is described oscillating with a mean frequency and its coherence is given by the magnitude of a (mean-field) order parameter, an approach analogous to the Eulerian description in hydrodynamics. Since then this approach has been successful in analytical investigations [2–9]. In contrast, accurate results for the finite-size Kuramoto model remain a challenge due to the great number of equations involved, nevertheless, the dynamics is richer. While in the case of global coupling, the full synchronization is the only stable equilibrium, in different topologies of the Kuramoto model multistability is allowed [10]. And, sustained by Lyapunov function argument, the system would reach an equilibrium state as $t \to \infty$ [11]. In this context, equilibriums play a central role in network dynamics.

Multistability [12–14], basin of attractions [15,16], and traveling waves [17] are some of the fundamental phenomena directly related with equilibriums in vari-

ants of the Kuramoto model with both attractive and repulsive phase couplings.[1] These phenomena are also observed in real-world networks [18–21]. Such manifestations are mostly studied in the continuous thermodynamic limit and keep not yet well understood. Exact solutions for a lower number of oscillators in the Kuramoto model are mandatory in this study, but they are still a topic of investigation [22,23].

To shed some light on those problems, we study the Kuramoto–Sakaguchi (KS) model [24], a generalization of the Kuramoto model, explicitly for a finite number of N identical oscillators symmetrically coupled ($G = G^T$, in matrix representation). For an approach to the skew-symmetric coupling ($G = -G^T$), the complementary case,[2] we point out Ref. [25]. Whereas, in that work, the authors studied the role of the coexistence of Hamiltonian-like and dissipative behaviors, here we explore the dynamics of oscillators in the phase and parameter spaces. In contrast to traditional investigations, where the time evolution of the network is followed by the order parameter [8], we obtain solutions describing precisely the individual trajectory of each oscillator when the system is close to an equilibrium, in some sense similar to the Lagrangian description in hydrodynamics. We present several numerical studies in great accordance with our theory. Our goal is to give theoretical support for phenomena of synchronization observed in real-world networks with more complex phase oscillators. In fact, synchronizations in the repulsive regime discussed in this work were recently observed in a nice experimental network of nanoelectromechanical oscillators [26]. In the analysis, the authors show that for first-order expansion in the coupling parameter, their model can be represented by the Kuramoto–Sakaguchi network model. For stronger couplings, terms of second-order of the expansion dominate and different behaviors take place delimiting the boundary of our theoretical predictions.

In the KS model, the time evolution of each phase oscillator is governed by

$$\dot{\theta}_{\mathrm{x}} = \omega_{\mathrm{x}} + \sum_{\langle \mathrm{y}, \mathrm{x} \rangle} G(\mathrm{x}, \mathrm{y}) \sin\left(\theta_{\mathrm{y}} - \theta_{\mathrm{x}} - \alpha\right), \qquad (1)$$

---

[1] The dynamic of networks with repulsive phase couplings is almost unknown in spite of its relevance in neurons networks. In the repulsive regime, the oscillators do not collapse in a single phase although they synchronize in frequency.

[2] Recalling that a matrix $M_{N \times N}$ can be written by a combination of symmetric and skew-symmetric matrices.

where $\mathrm{x} = 0, 1, 2, \ldots, N - 1$ identifies the xth oscillator in a ring, ω_{x}, its natural frequency, and $G(\mathrm{x}, \mathrm{y})$, the coupling rule between it and the yth oscillator. The notation $\langle \mathrm{y}, \mathrm{x} \rangle$ means that the summation is on the R nearest neighbors in both sides of oscillator x, then y assumes the values $\mathrm{x} - R, \mathrm{x} - R + 1, \ldots, \mathrm{x}, \ldots, \mathrm{x} + R$, where R can be from $R = 1$ (*local* coupling) to $R = (N - 1)/2$ (*global* coupling), if N is odd. If $1 < R < (N - 1)/2$ the coupling is called *nonlocal*. Finally, $\alpha \in (-\pi, \pi]$ is a constant that, for positive coupling G, determines the regime of the network named *attractive* if $|\alpha| < \pi/2$ and *repulsive* otherwise. In the attractive regime, the state where all oscillators have the same phase is allowed, contrary to the repulsive regime [27]. Further, the eigenvalue expression obtained in Eq. (11) and its applications in Fig. 3 as well as in Table 1 will make this notion more precise.

Considering N identical oscillators ($\omega_{\mathrm{x}} = $ constant, $\forall \mathrm{x}$) interacting according to KS model, with periodic boundary conditions, as in general studies of chimera states [28–30] (for the case $\omega_{\mathrm{x}} \neq \omega_{\mathrm{y}}$ see [23]), an equilibrium is related to the phase difference between the nearest neighbors of oscillators $\Delta = \theta_{\mathrm{x}+1} - \theta_{\mathrm{x}}$. Due to the similarity, any homogeneous phase distribution of the oscillators along a circle is an equilibrium, i.e.,

$$\Delta = \frac{2\pi}{N} q, \qquad q = 0, 1, 2, \ldots, N - 1. \qquad (2)$$

The integer q denotes the number of loops needed to distribute the phase oscillators in the circle. The trivial solution is $\Delta = 0$ (or 2π) corresponding to the full synchronization. For the rest ($q \neq 0$), we say that the network is synchronized in a *q-twisted state*. Note that there is no different distribution for $q \geq N$.

In this work, we describe the stability properties of the q-twisted states assuming a general symmetric coupling $G(\mathrm{x}, \mathrm{y})$, only dependent on the absolute distance between oscillators – i.e., $G(\mathrm{x}, \mathrm{y}) = G(|\mathrm{y} - \mathrm{x}|) \equiv G_n = G_{-n}$, for distance given by $n = \mathrm{y} - \mathrm{x}$. More specifically, we determine the set of eigenvalues associated with each state identifying the complete stability scenario of hyperbolic and non-hyperbolic equilibriums for a finite number N of oscillators. As an application, we show specifically this scenery in the parameter space $R \times q$ of the repulsive regime and calculate the bifurcation of twisted states in the thermodynamic limit. Here, we apply the theory in numerical experiments implemented with the traditional coupling

G_n = constant. Nevertheless, we have considered different couplings as exponential [$G_n \propto \exp(-k|n|)$] and cosine [$G_n \propto 1 - A\cos(n)$], assumed in the seminal works about chimera [28,31], and also obtained great accordance with the theory. Nevertheless, we point out that the closer the dynamics is to equilibrium the better the theory works. For longer distances, our analytical results fail to describe trajectories but can help to describe global behaviors.

In the end, we discuss how these results contribute to a dynamical interpretation of chimera states.

2 Theory

2.1 Synchronization frequency

Without loss of generality, we assume that frequency $\omega_x = 0$, periodic boundary conditions ($\theta_0 = \theta_N$) and N odd. Then, Eq. (1) can be rewritten as

$$\dot{\theta}_x = \sum_{n=-R}^{R} G_n \sin(\theta_{x+n} - \theta_x - \alpha). \tag{3}$$

Based on the system symmetry, we assume that the network shall asymptotically converge to a q-twisted state with the same constant frequency $\dot{\theta}_x = \Omega$. Assuming $\theta_0 = 0$, we obtain $\theta_x = \Omega t + \Delta x$. Substituting this result in Eq. (3), the network synchronization frequency Ω of any mode q is obtained:

$$\Omega = \sum_{n=-R}^{R} G_n \sin(n\Delta - \alpha). \tag{4}$$

2.2 Stability of q-twisted states

We begin to analyze the stability of q-twisted states by taking into account a small perturbation in its solution: $\theta_x = \Omega t + \Delta x + \mathcal{E}_x$. Then,

$$\dot{\theta}_x = \Omega + \dot{\mathcal{E}}_x. \tag{5}$$

Substituting Eq. (5) in the LHS of Eq. (3) and expanding the (perturbed) RHS of Eq. (3) to first-order in $\mathcal{E}_x$, we obtain (with $\psi \equiv n\Delta - \alpha$)

$$\dot{\mathcal{E}}_x(t) = \sum_{n=-R}^{R} G_n [\mathcal{E}_{x+n}(t) - \mathcal{E}_x(t)] \cos\psi. \tag{6}$$

With the ansatz $\mathcal{E}_x(t) = \mathcal{A}_x e^{\lambda t}$, (or with vector notation: $\boldsymbol{\mathcal{E}}(t) = \boldsymbol{\mathcal{A}} e^{\lambda t}$), Eq. (6) becomes

$$\lambda \mathcal{A}_x = \sum_{n=-R}^{R} G_n [\mathcal{A}_{x+n} - \mathcal{A}_x] \cos\psi$$

$$= \sum_{n=1}^{R} G_n [\rho_n \mathcal{A}_{x-n} + \mu_n \mathcal{A}_{x+n}] - \beta \mathcal{A}_x, \tag{7}$$

where $\rho_n = \cos(n\Delta + \alpha)$, $\mu_n = \cos(n\Delta - \alpha)$, and

$$\beta = \sum_{n=1}^{R} G_n(\rho_n + \mu_n) = 2\cos\alpha \sum_{n=1}^{R} G_n \cos(n\Delta). \tag{8}$$

Then, Eq. (7) can be written in the matrix form $\lambda \mathbf{A} = M\mathbf{A}$, where $\mathbf{A} = [\mathcal{A}_0, \ldots, \mathcal{A}_x, \ldots, \mathcal{A}_{N-1}]^T$ and M is a circulant matrix [32]

$$M = \begin{pmatrix} -\beta & G_1\mu_1 & G_2\mu_2 & \cdots & G_2\rho_2 & G_1\rho_1 \\ G_1\rho_1 & -\beta & G_1\mu_1 & \cdots & G_3\rho_3 & G_2\rho_2 \\ G_2\rho_2 & G_1\rho_1 & -\beta & \cdots & G_4\rho_4 & G_3\rho_3 \\ \vdots & \vdots & \vdots & \vdots & \ddots & \vdots \\ G_1\mu_1 & G_2\mu_2 & G_3\mu_3 & \cdots & G_1\rho_1 & -\beta \end{pmatrix} \tag{9}$$

with (non-normalized) eigenvectors given by

$$\mathbf{A}_\ell = \left[z_\ell{}^0, \ldots, z_\ell{}^x, \ldots, z_\ell{}^{N-1} \right]^T,$$
$$z_\ell \equiv \exp\left(i\frac{2\pi}{N}\ell \right), \tag{10}$$

with $\ell = 0, 1, 2, \ldots, N - 1$.

The ℓth eigenvalue of the q-twisted state is given by $\lambda_\ell = \gamma_\ell + i\varpi_\ell$, with

$$\gamma_\ell = -4\cos\alpha \sum_{k=1}^{R} G_k \cos\left(k\frac{2\pi}{N}q \right) \sin^2\left(k\frac{\pi}{N}\ell \right) \tag{11}$$

$$\varpi_\ell = 2\sin\alpha \sum_{k=1}^{R} G_k \sin\left(k\frac{2\pi}{N}q \right) \sin\left(k\frac{2\pi}{N}\ell \right). \tag{12}$$

Any perturbation $\boldsymbol{\mathcal{E}}(t)$ can be written in terms of the eigenmodes: $\boldsymbol{\mathcal{E}}(t) = \sum_\ell C_\ell \mathbf{F}_\ell(t)$, with $\mathbf{F}_\ell(t) = \mathbf{A}_\ell e^{\lambda_\ell t}$ or, without vector notation, $\mathcal{E}_x(t) = \sum_\ell C_\ell F_\ell$ (x, t) where $F_\ell(x, t) = z_\ell{}^x e^{\lambda_\ell t}$ is a wave function:

$$F_\ell(x, t) = e^{\gamma_\ell t} \exp\left(i\left(\frac{2\pi\ell}{N}x + \varpi_\ell t \right) \right). \tag{13}$$

Notice that the eigenmode $\ell = 0$, with eigenvalue $\lambda_0 = 0$ and eigenvector $\mathbf{A}_0 = [1, 1, \ldots, 1]^T$, results from the invariance of the system given Eq. (1) under a global phase shift $\theta_x \to \theta_x + C$, $\forall x$. Then, despite of the N equations following Eq. (1), the equilibriums are $(N-1)$-dimensional since they are related to the phase difference. In other words, the sum of all phase differences is a multiple of 2π due to the periodic boundary condition such that any phase difference can be obtained from the others $N-1$. Therefore, the eigenmode $\ell = 0$ shall be disregarded below.

3 Applications in finite networks

3.1 Long-lived eigenmodes

In general, attractive and repulsive regimes are studied for $\alpha = 0$ and π, respectively. The convergence to any q-twisted state is monotonically exponential, missing the effect of the complex part of the eigenvalues [Eq. (12)] in the dynamics. For different values of α, according to our results, the behavior close to equilibriums is more interesting. Except for the state $q = 0$, where nothing changes ($\varpi_\ell = 0$), all eigenmodes can oscillate with their particular frequencies given by Eq. (12). To test this prediction, we confronted them with some "brute force" numerical simulations. In one of many simulations, we evolved a network of 50 oscillators locally coupled ($R = 1$) with $\alpha = 1.5$ and $G_n = 0.1$. The time evolution of such a system was performed by direct numerical integration of the 50 differential equations [Eq. (3)] from random initial conditions and the system reached a twisted state with $q = 8$: the system has frequency synchronization, i.e., all the oscillators have the same phase velocity $\Omega = -0.20665$, and the phase difference between any two neighbors is $\theta_{x+1} - \theta_x = 8(2\pi/50)$, $\forall x$.

Regarding the theoretic aspect, for $q = 8$, we can compute all the (real part of) eigenvalues (only for $\ell > 0$) with Eq. (11):

$$\gamma_1 = \gamma_{49} \approx -0.598 \times 10^{-4},$$
$$\gamma_2 = \gamma_{48} \approx -2.38 \times 10^{-4},$$
$$\gamma_3 = \gamma_{47} \approx -5.32 \times 10^{-4},$$
$$\cdots$$
$$\gamma_{24} = \gamma_{26} \approx -151. \times 10^{-4},$$
$$\gamma_{25} \approx -152. \times 10^{-4}.$$
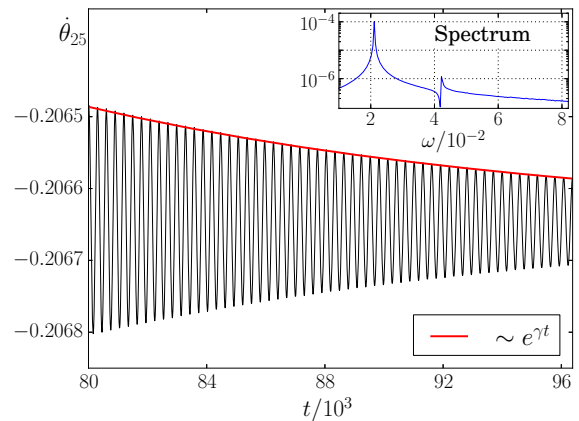
Fig. 1 Behavior of $\dot{\theta}_{25}$ in the KS model for local coupling (black). The exponential decreasing curve (red) and the spectrum (blue) demonstrate the behavior of the longest-lived eigenmodes of the 8-twisted state. $N = 50$, $R = 1$, $\alpha = 1.5$, and $G_n = 0.1$. (Color figure online)

We observe that all $\gamma_{\ell(>0)}$ are negative and, as we shall discuss in the next subsection, it is a clear signal that the 8-twisted state is stable, in agreement with the numerical simulation. On the other hand, if we assume that the lifetime of an eigenmode can be estimated as $\tau_\ell \propto |\gamma_\ell|^{-1}$, clearly the eigenmodes $\ell = 1$ and 49 have the longest lifetimes.

For large times, but before the system reaches the final state $q = 8$, it is reasonable to expect a behavior dominated by the eigenmodes $\ell = 1, 49$ of the 8-twisted state: a wave [Eq. (13)] with amplitude decaying exponentially with constant $\gamma = \gamma_{1,49} < 0$. Substituting the parameters of the network in Eqs. (4, 12), we obtain, respectively, $\Omega_8 = -0.20665$ and $\varpi_1 = |\varpi_{49}| = 0.0211 \equiv \omega_T$.

In Fig. 1, we show the behavior of $\dot{\theta}_{25}$ (the phase velocity of the oscillator in the site $x = 25$) for $80{,}000 \le t \lesssim 96{,}000$ (black line) and its corresponding spectrum. One can observe in Fig. 1 that the pronounced peak in the spectrum is around $\omega \approx \omega_T$ (blue line) and the oscillation amplitude of $\dot{\theta}_{25}$ is decaying exponentially to the final synchronization frequency Ω_8 as predicted above: the red curve is obtained with a function proportional to $\exp(\gamma t)$.

We present also the spectrogram for $\dot{\theta}_{25}$ in Fig. 2, one can observe that initially the oscillator $x = 25$ has several frequencies with high amplitude. This is because, due the random initial conditions, the network is deciding in which one of the 25 attractors ($|q| \le 12$) it will converge. Following, just some frequencies
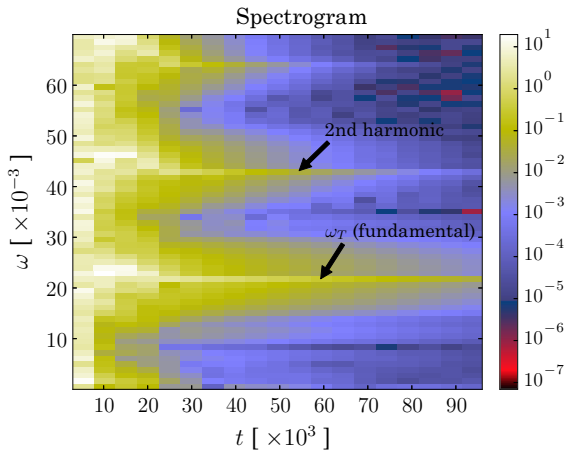
Fig. 2 Spectrogram of $\dot{\theta}_{25}$

survived, the system decided to the twisted state $q = 8$ ($\Omega_8 \approx -0.20665$). Now, we only observe oscillations of its eigenmodes given by ϖ_ℓ with $\ell = 1, \ldots, N-1$ (Eq. (12)). Then, all eigenmodes die one by one, being ω_T the last one.

3.2 Multistability

The eigenmodes[3] are stable if $\gamma_\ell < 0$ and unstable if $\gamma_\ell > 0$. Thus, a q-twisted state can be classified as:

(a) **a**ttractor (hyperbolic) if $\gamma_1, \ldots, \gamma_{N-1} < 0$;
(b) **r**epeller (hyperbolic) if $\gamma_1, \ldots, \gamma_{N-1} > 0$;
(c) **s**addle (hyperbolic) if $\exists \, \gamma_\ell \gamma_{\ell'} < 0$;
(d) **n**on-hyperbolic if $\exists \, \gamma_\ell = 0$.

We call the attention for some remarks about the items above. (i) If a non-hyperbolic state has all the other $\gamma_\ell < 0$, the system does not converge completely to the q-twisted state; however, in general, it synchronizes in frequency. We call this state as *neutrally* stable. In subsection "Hyperbolic $\times$ non-hyperbolic stable states," we discuss the different signatures of these equilibriums: the former has a homogeneous phase distribution ($\theta_{x+1} - \theta_x = $ constant, $\forall x$) and the latter does not have. (ii) Due to the assumption of periodic boundary conditions, there is a symmetry between the stability of $-q$ and q states: The real part of their eigenvalues [Eq. (11)] is the same ($\gamma_q = \gamma_{-q}$). One also can see from Eq. (2)

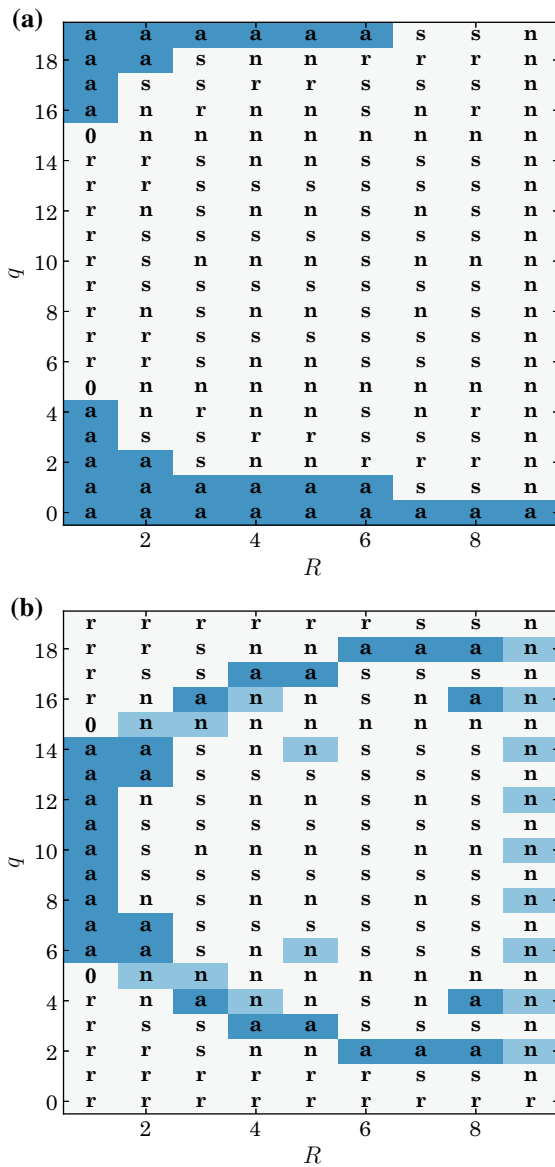[3] Remember that only the eigenmodes with $\ell > 0$ are considered here.

that $-q$ and $N - q$ represent the same state, so there is another way of labeling the twisted states, for instance: $q = -(N-1)/2, \ldots, -1, 0, 1, \ldots, (N-1)/2$, if N is odd. (iii) If $\alpha = \pi/2$ the eigenvalues are purely imaginary and the stability is not well defined by our assumptions. (iv) Since typically $\varpi_\ell \neq 0$, there are several different types of equilibriums with stable and unstable manifolds which we generically call saddle. (v) Although our deduction assumed N odd, the analysis can be easily extended to N even.

As an example, we consider a network of $N = 20$ oscillators in a ring with the same and positive coupling for attractive and repulsive regimes. We varied R from local to nonlocal and tested the stability of each q-twisted state according to the sign of γ_ℓ, $\forall \, \ell > 0$. The outcome is compiled in Fig. 3.

The **a**ttractors are represented by blue rectangles in the diagrams, and the neutrally (**n**on-hyperbolic) stable states are in light blue. While **r**epellers, **s**addles, and **n**on-hyperbolic unstable states are in white.

According to Eq. (11) and conditions (a-d) above, if we change the system from attractive to repulsive regime (or vice versa), repellers become attractors and vice versa, including non-hyperbolic equilibriums, and saddles keep their unstable character in both regimes. There are some non-hyperbolic states with stable and unstable manifolds. Close to these equilibriums, the dynamic is saddle-like and they are also unstable in both regimes. Finally, the states with '**0**' in Fig. 3 have $\gamma_\ell = 0$, $\forall \ell$ and our analysis above is unable to determine their stability. However, according to some simulations we performed, such states seem to be unstable in both regimes.

The stable states, highlighted in blue and light blue in our diagrams of Fig. 3, should be compared with those in Fig. 1 of Ref. [13], which were obtained exclusively by a large and intense work of "brute force" numerical integration of the Kuramoto equations. One can readily realize that the analysis performed here with the eigenvalues [Eq. (11)] provides simultaneously (i) a much faster (almost immediate) computational tool capable of producing (ii) a much more detailed scenario of the q-twisted states that identifies the different hyperbolic (repellers and saddles) as well as non-hyperbolic (neutrally stable and saddle-like) equilibriums, for any values of N and R. In contrast, the diagrams in Fig. 1 of Ref. [13] only show whether the pair (q, R) is stable or not.

(a)

q \ R	1	2	3	4	5	6	7	8	9
19	a	a	a	a	a	a	s	s	n
18	a	a	s	n	n	r	r	r	n
17	a	s	s	r	r	s	s	s	n
16	a	n	r	n	n	s	n	r	n
15	0	n	n	n	n	n	n	n	n
14	r	r	s	n	n	s	s	s	n
13	r	r	s	s	s	s	s	s	n
12	r	n	s	n	n	s	n	s	n
11	r	s	s	s	s	s	s	s	n
10	r	s	n	n	n	s	n	n	n
9	r	s	s	s	s	s	s	s	n
8	r	n	s	n	n	s	n	s	n
7	r	r	s	s	s	s	s	s	n
6	r	r	s	n	n	s	s	s	n
5	0	n	n	n	n	n	n	n	n
4	a	n	r	n	n	s	n	r	n
3	a	s	s	r	r	s	s	s	n
2	a	a	s	n	n	r	r	r	n
1	a	a	a	a	a	a	s	s	n
0	a	a	a	a	a	a	a	a	a

(b)

q \ R	1	2	3	4	5	6	7	8	9
19	r	r	r	r	r	r	s	s	n
18	r	r	s	n	n	a	a	a	n
17	r	s	s	a	a	s	s	s	n
16	r	n	a	n	n	s	n	a	n
15	0	n	n	n	n	n	n	n	n
14	a	a	s	n	n	s	s	s	n
13	a	a	s	s	s	s	s	s	n
12	a	n	s	n	n	s	n	s	n
11	a	s	s	s	s	s	s	s	n
10	a	s	n	n	n	s	n	n	n
9	a	s	s	s	s	s	s	s	n
8	a	n	s	n	n	s	n	s	n
7	a	a	s	s	s	s	s	s	n
6	a	a	s	n	n	s	s	s	n
5	0	n	n	n	n	n	n	n	n
4	r	n	a	n	n	s	n	a	n
3	r	s	s	a	a	s	s	s	n
2	r	r	s	n	n	a	a	a	n
1	r	r	r	r	r	r	s	s	n
0	r	r	r	r	r	r	r	r	r

Fig. 3 Stability diagrams of the q-twisted states for $N = 20$ oscillators equally coupled in a ring for **a** attractive regime ($|\alpha| < \pi/2$) and **b** repulsive regime ($\pi/2 < |\alpha| \leq \pi$). Highlight for stable states: (hyperbolic) **a**ttractors in blue, neutrally (**n**on-hyperbolic) stable states in light blue; **s**addles, **r**epellers and also **n**on-hyperbolic unstable states are in white. (Color figure online)

3.3 Bifurcations in the repulsive regime

Now, we analyze the case of a network of oscillators in the continuum limit. We also assume below that each oscillator is coupled to its R nearest neighbors (each side) with constant coupling.

We start with a network locally coupled ($R = 1$). From Eq. (11), the stability of a q-twisted state can change from attractor to repeller (vice versa) according to the sign of $\cos(2\pi q/N)$. For $|q| = N/4$, all eigenvalues are purely imaginary,[4] and consequently these states are not asymptotically stable or unstable, there is a bifurcation point given by the ratio $|q|/N = 1/4$. Since in our representation $|q| \leq (N-1)/2$, the maximum ratio $|q|/N$ tends to $1/2$ in the limit of $N \to \infty$. Therefore, a network locally coupled presents approximately half of its states as (hyperbolic) attractors and the other half, repellers, independently of α and G_n.

For nonlocal couplings, the stability of the q-twisted states depends only on the ratio R/N. This is clearly expressed in the thermodynamic limit $N \to \infty$ of Eq. (11) where, in the attractive regime, stable solutions are obtained when

$$\int_0^{R/N} \cos(2\pi q z) \sin^2(\pi \ell z)\, \mathrm{d}z > 0 \tag{14}$$

in the range $1 \leq R \leq N/2$, for $G_n > 0$ and constant. For a given q-twisted state, its stability changes when the integral in the inequality (14) is null. Defining the function $f(x, y) \equiv \sin(2\pi xy)/y$, with $x = R/N$, to express the solution of the integral, the bifurcation condition is given by

$$f(x, (\ell - q)) - 2f(x, q) + f(x, (\ell + q)) = 0. \tag{15}$$

For a chosen q, we set $\ell = 1$ and vary x from 0 to 0.5 and find values ($x_{q(\ell=1)}$) that solve the equation. This process should be repeated for $\ell = 2, 3, \ldots$. Since the stability condition Eq. (14) is satisfied when $x \gtrsim 0$, a q-twisted state loses its stability when Eq. (15) is satisfied for some ℓ, remaining unstable in the rest of the range of x. In our example, twist bifurcations happen for $\ell = 1$: $tb_{q(1)} = x_{q(1)}$ (See the middle column in Table 1). This result is valid for more complex networks. In [10], the authors obtained the same solution from the mean-field approach considering a symmetric distribution of coupling G_n.

In the repulsive regime, the condition of stability is no longer satisfied when $x \gtrsim 0$ for nonlocal couplings. So, now, the first twist bifurcation point demarcates

---

[4] A good example can be seen in the first column of both diagrams in Fig. 3, the states $q = 5$ and $q = 15$ (which in turn is equivalent to the state $q = -5$) has $\gamma_\ell = 0$, $\forall \ell$.

Table 1 Bifurcations in the continuum limit

Twisted state	Attractive regime (**I**)		Repulsive regime (**II**)	
q	ℓ	$tb_{q(\ell)}$	ℓ	$tb_{q(\ell)}$
1	1	0.340461	–	Unstable
2	1	1/6	5	0.277562
3	1	0.110727	7	0.191433
			5	0.308065
4	1	0.082948	9	0.145507
			7	0.225577
			2	5/12
5	1	0.066323	11	0.117041
			9	0.178895
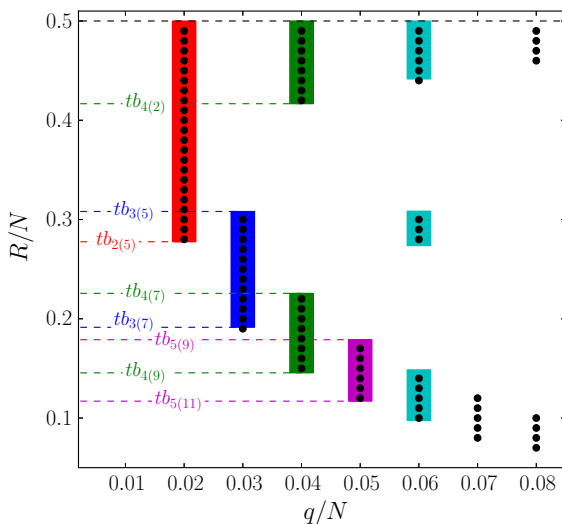
Fig. 4 Stability in the repulsive regime. Black dots are the stable states for $N = 100$. Colored stripes are regions (in the continuum limit) where q-twisted states are expected to be stable, according to table 1 (For comparison, the values of q/N were calculated with $N = 100$ in both cases.). (Color figure online)

the boundary where a q-twisted state becomes stable. In this regime, several twist bifurcation can occur as shown in the last column of Table 1. For local couplings, the condition becomes $|q|/N > 1/4$.

For any value of R/N, the state of full synchronization ($q = 0$) shall be a hyperbolic attractor in the attractive regime and a hyperbolic repeller in the repulsive regime. On the other hand, the numbers in table 1 should be interpreted as follows: (**I**) In the attractive regime, $tb_{q(1)}$ is the highest value of R/N where the q-twisted state is stable. For instance, $tb_{2(1)} = 1/6$ means that the state $q = 2$ is stable for $0 < R/N < 1/6$. (**II**)

In the repulsive regime, several values of $tb_{q(\ell)}$ determine ranges of stabilities, for a given q. For instance: $q = 4$ is stable when $tb_{4(9)} < R/N < tb_{4(7)}$ and $tb_{4(2)} < R/N < 0.5$ (green stripes in Fig. 4).

In Fig. 3 and also Table 1, where $G_n > 0$, the distinction between the attractive and repulsive regimes becomes clearer: for $|\alpha| < \pi/2$, the fully synchronized state (all phases equal or $q = 0$) is an attractor for all values of R and for $R/N \gtrsim 0.34$ only the state $q = 0$ is an attractor. With $\pi/2 < |\alpha| \leq \pi$, the state $q = 0$ is a repeller for any value of R. The network will synchronize in frequency, but with different values for the phases.

3.4 Dynamics close to equilibrium

3.4.1 Close to an attractor

It is important to remember that our analysis of stability was performed by taking into account a small perturbation $\mathcal{E}_x$ in the q-twisted states. On the other hand, with the (real part of the) eigenvalues Eq. (11), one can predict if a given q-twisted state is stable or not, then if the system is close to a stable state, the time evolution of each phase can be approximately

$$\theta_x(t) \approx \Omega t + \Delta x + \sum_\ell C_\ell F_\ell(x, t), \quad (16)$$

where Ω is the synchronization frequency of the state, given by Eq. (4); $\Delta = 2\pi q/N$ and $F_\ell(x, t)$ are the (perturbation) eigenfunctions Eq. (13). Eventually, the time evolution of the Kuramoto order parameter, for a system close to an attractor, could be predicted directly with our formulas:

$$\rho(t) = \left| \frac{1}{N} \sum_x e^{i\theta_x(t)} \right|. \quad (17)$$

We considered a system with parameters $\alpha = 0.4$, $R = 1$, $N = 50$, $G_n = 1/50$ and initially in the state $q_0 = 0$, (then $\Delta = 0$, $\forall x$), with a not too small perturbation:

$$\theta_x(0) = 1.4 \exp\left[-\frac{(x - 25)^2}{200} \right] \sin\left(\frac{7.5\pi}{50} x \right), \quad (18)$$

with $x = 0, 1, \ldots, 49$, see Fig. 5a.

(a)

(b)
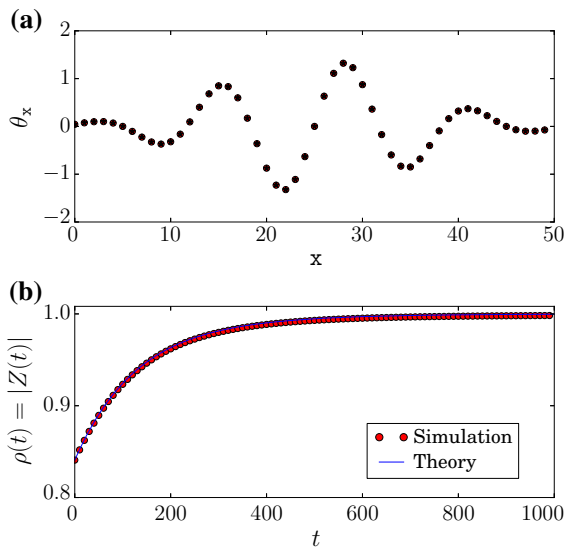
Fig. 5 **a** initial configuration of phases, given by Eq. (18); **b** comparison between the theoretical prediction (obtained with Fourier decomposition and our equations for perturbations, blue curve) and the results obtained by direct numerical integration of 50 differential equations (red circles). (Color figure online)

From the condition above, we evaluated the phases by (i) "brute force" numerical integration of the 50 (KS) differential equations and by (ii) our theoretical formulation: the initial condition Eq. (18) was decomposed in its Fourier components A_ℓ, B_ℓ; Ω and the eigenvalues were obtained with Eqs. (4, 11, 12) for $q = 0$; and the time evolution of each phase was calculated with:

$$\theta_x(t) = \Omega t + \sum_\ell e^{\gamma_\ell t} \left[A_\ell \cos \left(\frac{2\pi\ell}{50} x + \varpi_\ell t \right) \right.$$
$$\left. + B_\ell \sin \left(\frac{2\pi\ell}{50} x + \varpi_\ell t \right) \right]. \quad (19)$$

Then, the Kuramoto order parameter was computed for both cases and the comparison is presented in Fig. 5b. One can observe that both results start equals and they diverge slightly as the network evolves. This is due to a delay introduced by our analytical evolution caused by the distance that the initial condition is from the equilibrium $q = 0$.

3.4.2 Close to a repeller

We studied the behavior close to a repeller, while the system moves away from it, through one eigendirection of its unstable manifold. We considered a network of

(a)

(b)
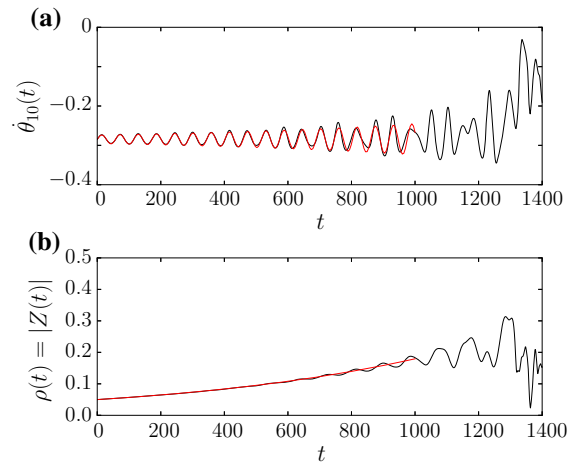
Fig. 6 Initial time evolution of: **a** The phase velocity of the oscillator in $x = 10$; **b** the order parameter ρ. Black curves were obtained by direct integration (Runge–Kutta) of the 20 KS equations. In turn, the red curves were obtained with our approximation, Eqs. (17,21). (Color figure online)

$N = 20$ phase oscillators with $R = 3$, $G_n = 1/20$, $\alpha = 1.6 > \pi/2$ (repulsive regime) and with initial condition close to equilibrium $q = 1$. In Fig. 3b, we can observe that $q = 1$ is a repeller.

The initial condition for the phases is $q = 1$ plus a small perturbation ($A = 0.1$) in the eigenmode $\ell = 1$.

$$\theta_x(t = 0) = \left(\frac{2\pi}{20} \right) x + A \cos \left(\frac{2\pi}{20} x \right) . \quad (20)$$

On the other hand, with equations (4,11,12), one can obtain $\Omega_{(q=1)} \equiv \Omega_1 \approx -0.2847$ and the real and imaginary parts of the eigenvalue of mode $\ell = 1$: $\gamma_1 = 0.001295$, $\varpi_1 = 0.1095$. Then, the initial evolution of the phase oscillators can be approximated by

$$\theta_x(t) = \Omega_1 t + \left(\frac{2\pi}{20} \right) x + A e^{\gamma_1 t} \cos \left(\frac{2\pi}{20} x + \varpi_1 t \right) , \quad (21)$$

as can be observed in Fig. 6. By deriving Eq. (21), we obtained the phase velocity nearby the repeller (red line in Fig. 6a), we compared this with the direct result of numerical integration of the 20 KS equations (black curve). The behavior of the order parameter is presented in Fig. 6b, one can observe that Eqs. (17, 21) also provide a good approximation for the initial time, during which the system moves away from the repeller.

3.4.3 Close to a saddle

We also investigated the behavior close to a saddle, and we observed the system approaching it through one eigendirection of its stable manifold and after that moving away from it through its unstable manifold.

For this, we considered again a network of $N = 20$ phase oscillators, but with $R = 6$, $G_n = 1/20$, $\alpha = 1.6 > \pi/2$ (repulsive regime) and with initial condition close to equilibrium $q = 4$. In Fig. 3b, we can observe that for $R = 6$, the state $q = 4$ is a saddle.

The initial condition for the phases is $q = 4$ plus a small perturbation ($A = 0.1$) in the eigenmode $\ell = 16$, with eigenvalue $\lambda_{16} = \gamma_{16} + i\varpi_{16}$, where $\gamma_{16} = -0.006676$, $\varpi_{16} = -0.3403$,

$$\theta_x(t = 0) = \left(\frac{2\pi.4}{20}\right)x + A\cos\left(\frac{2\pi.16}{20}x\right) \quad . \quad (22)$$

Again, we integrated the 20 KS equations with the initial condition described above and observed the phase velocity of the oscillator in $x = 10$, $\dot{\theta}_{10}$, as shown in Fig. 7. Such variable has exponentially decreasing oscillations toward the state $q = 4$ and can be well approximated by (red curve in Fig. 7b)

$$\dot{\theta}_{10}(t) = \Omega_4 + Ae^{\gamma_{16}t}\left[\gamma_{16}\cos\left(\frac{2\pi.16}{20}10 + \varpi_{16}t\right) - \varpi_{16}\sin\left(\frac{2\pi.16}{20}10 + \varpi_{16}t\right)\right], \quad (23)$$

where $\Omega_4 \approx -0.08087$ is the synchronization frequency of $q = 4$. That is a clear signature of the system moving through the eigendirection of the stable manifold.

Before $t \sim 10^3$, $\dot{\theta}_{10}$ begins to oscillate with different frequency and exponentially increasing amplitude. Such behavior can be well approximated by the eigenmode $\ell = 12$, the blue curve in Fig. 7b is written as:

$$\Omega_4 + Be^{\gamma_{12}(t-t')}\cos(\varpi_{12}(t - t')), \quad (24)$$

where $\gamma_{12} = 0.001632$, $\varpi_{12} = -0.0588$ and the other constants: $B = 0.000642$ and $t' = 1011.4$.

3.5 Hyperbolic × non-hyperbolic stable states

Technically, the difference between hyperbolic (attractor) and non-hyperbolic (neutrally) stable states is the
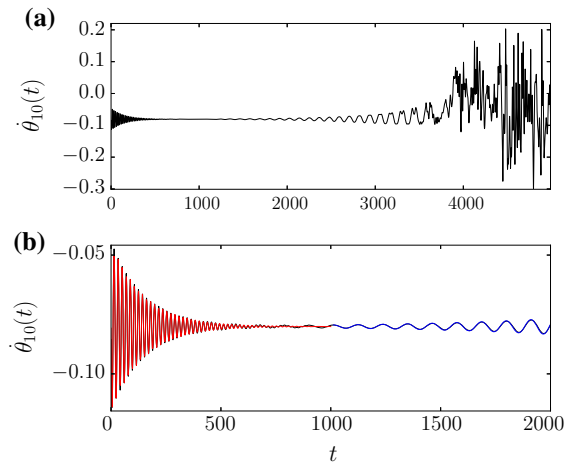
Fig. 7 Time evolution of phase velocity of the oscillator in $x = 10$. Black curves in **a** and **b** were obtained by direct integration (Runge–Kutta) of the 20 KS equations near a saddle; **b** red and blue curves: our approximations given by Eqs. (23) and (24). (Color figure online)

presence of at least one null eigenvalue in the latter case. The purpose of this section is to illustrate the role of the corresponding eigenvector in the dynamics of networks. To this end, we retake the network studied in section "Multistability" and focus in the 2-twisted state in the repulsive regime. We recall that for $R = 8$ and $R = 9$ this state is an attractor and neutrally stable, respectively (Fig. 3b).

Our experiment is based on a numerical integration (Runge–Kutta, with step size $\delta t = 2.5 \times 10^{-2}$ and 2×10^5 iterations) for each case ($R = 8$ and $R = 9$), with the same initial conditions close to the equilibrium ($q = 2$),

$$\theta_x(0) = x\frac{2\pi}{20}2 + r_x, \quad x = 0, 1, \ldots, 19, \quad (25)$$

where $r_x \in [-0.4, 0.4]$ is a random number. $G_n = 1/20$ and $\alpha = \pi$ are fixed, so that, the only difference between both simulations is the number of nearest neighbors R. The circles in Fig. 8a represent the initial conditions of all oscillators. In Fig. 8b, the squares represent the asymptotic state of the attractor for the coupling $R = 8$. All the oscillators are synchronized in frequency, and the phase distance between neighboring oscillators is the same constant $\Delta = 2\pi 2/20 = \pi/5$, corresponding to $q = 2$, as expected. Despite of this fact, the final state for $R = 9$ violates the assumption Eq. (2) about the phase distribution as the triangles
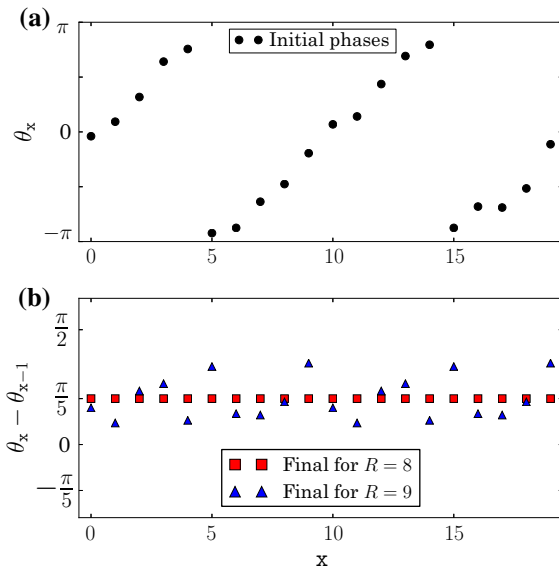
Fig. 8 Signatures of hyperbolic ($R = 8$) and non-hyperbolic ($R = 9$) stable states with $N = 20$, $\alpha = \pi$, $G_n = 1/20$, and $q = 2$. **a** Initial condition. **b** Final configurations for hyperbolic (red squares) and non-hyperbolic (blue triangles) stable states, both obtained numerically from the same initial condition (**a**). (Color figure online)

in Fig. 8b show. Nevertheless, the oscillators are synchronized in frequency ($\dot{\theta}_x = \Omega = 0$, $\forall x$) and with $\bar{q} \equiv \sum_x (\theta_x - \theta_{x-1})/(2\pi) = 2$. That is the feature of neutral stability.

It is worth to mention that in our simulations we have not seen a distribution devoid of symmetry in neutrally stable states. Note that in Fig. 8b the sequence of triangles for $x = 0$ to $x = 9$ is repeated from $x = 10$ to $x = 19$. Moreover, that is not the only solution. Different initial conditions lead the system to different configurations around the neutrally stable state.

Concerning the eigenvectors, stable hyperbolic equilibriums present all of them associated with negative eigenvalues. The dimensions of the phase space and the stable manifold are the same at the equilibriums attracting exponentially trajectories to the equilibrium state. In its turn, neutrally (non-hyperbolic) stable equilibriums present eigenvectors corresponding to negative and null eigenvalues giving rise to stable and center manifolds, respectively. The space, close the equilibriums, splits into three different behaviors: trajectories in the stable manifold converge to the equilibrium, in the center manifold they move slowly until they stop without reaching the equilibrium, and trajectories out of these manifolds are attracted to the center manifold,

due to the action of the stable manifold, ceasing the movement. Linear analyses are not able to determine this behavior; nevertheless, our simulations indicate that the dynamic stops close to such non-hyperbolic equilibriums.

4 Final remarks

In this work, we presented the exact solution of the KS model for finite N number of identical oscillators symmetrically coupled and give an extended analysis about the stability and the dynamics close to the q-twisted states. With that, we can characterize precisely the nature around attractors, repellers, saddles, and also non-hyperbolic equilibriums, some of the well known most fundamental invariant sets capable of dictating the global behavior in dynamic systems. We expect that this study gives new insights to understand several basic open problems in synchronization. Here, we give an example. It is known that in KS models a chimera state (simultaneous manifestation of coherent and incoherent states in a network) collapses to $q = 0$ (full synchronization) state after some time. In order to increase the lifetime without increasing the network, the relation $R/N \approx 0.35$ has been largely employed, seemingly empirically, in studies of chimera states in KS model and several others different network models based on Rössler, Lorenz, FitzHugh-Nagumo, Stuart-Landau, and Mackey-Glass dynamical systems [33–35].

According to our results, the bifurcations presented in table 1 indicate that for $R/N \gtrsim 0.34$ only the state $q = 0$ is stable. The other states are unstable, mostly saddle(-like) and some repellers. While the equilibrium $q = 0$ keeps some oscillators synchronized, the structure of the unstable equilibriums contributes globally to the incoherent behavior as follows: First, we notice that in chimera studies it is usual to set $\alpha \lesssim \pi/2$. Observe that the real part of the eigenvalues [Eq. (11)], for $\alpha \approx \pi/2$, indicates that the lifetime $\tau_\ell \propto |\gamma_\ell|^{-1}$ is very large, since $\gamma_\ell \propto \cos\alpha$. It promotes slow relaxation of all eigenmodes. On the opposite side, the complex part of the eigenvalues [Eq. (12)] is maximized, in view that $\varpi_\ell \propto \sin\alpha$. So that, there are $(N-1)$ different frequencies of oscillations for each one of the $(N-1)$ q-twisted states (the state $q = 0$ does not present oscillations in its eigenmodes). Therefore, in the chimera state of the KS model, there are poten-

tially $(N-1)^2$ perturbing waves [Eq. (13)], arisen at the unstable equilibriums, traveling globally along the incoherent oscillators of the network.

Additionally, enhancing proportionally N and R, fixing the ratio $R/N \gtrsim 0.34$, there will appear new populations of saddles increasing, even more, the ergodicity of the environment. The phase of the oscillators will keep being attracted and repelled by the stable and unstable manifolds from one equilibrium to another indefinitely extending the chimera lifetime. For a deeper description of chimera states, one should also analyze the dynamical behavior of collective variables with Ott-Antonsen or Watanabe-Strogatz methods beyond others; however, our scenery described above is at least qualitatively consistent with the previous numerical study of KS model for $R/N \approx 0.35$ and $\alpha = 1.46$ [36]. The authors, in this work, also observed that the average lifetime of chimeras (before the full synchronization of the network) grows exponentially with N.

Another novelty from our results concerns the repulsive regime of the KS model. Much attention has been paid to the full synchronization in networks, nevertheless bird flocks, fish schools, activity of cortical neurons in cats, and traveling waves in undulatory locomotion of fishes and lampreys are some of several manifestations in nature strongly related with a kind of synchronization where, contrary to the full synchronization and as in the repulsive regime of the KS model, the units must not approach each other indefinitely. They converge asymptotically to different states resulting in a homogeneous distribution, crucial for the efficient operation of the network. It is impressive that despite several important advances performed in the paradigmatic KS model its repulsive regime remained almost untouched. With the analysis presented, this work raises the knowledge about the repulsive regime to the same level of the (traditional) attractive regime concerning the equilibrium states.

Finally, as a recent example of the relevance of eigenvalues in the Kuramoto model, despite the complexity of the basin of attraction boundary [37], the statistical size of the basin of attraction of twisted states can be estimated by their eigenvalues, indicating that global phenomena can be understood by local studies in networks of phase oscillators [38].

Compliance with ethical standards

References

1. Kuramoto, Y.: Self-entrainment of a population of coupled non-linear oscillators. In: International Symposium on Mathematical Problems in Theoretical Physics, p. 420. Springer, Berlin (1975)
2. Kuramoto, Y.: Chemical Oscillations, Waves, and Turbulence. Springer, Berlin (1984)
3. Watanabe, S., Strogatz, S.H.: Integrability of a globally coupled oscillator array. Phys. Rev. Lett. **70**, 2391 (1993)
4. Strogatz, S.H.: From Kuramoto to Crawford: exploring the onset of synchronization in populations of coupled oscillators. Physica D **143**, 1 (2000)
5. Strogatz, S.H.: Exploring complex networks. Nature **410**, 268 (2001)
6. Acebrón, J.A., Bonilla, L.L., Vicente, C.J.P., Ritort, F., Spigler, R.: The Kuramoto model: a simple paradigm for synchronization phenomena. Rev. Mod. Phys. **77**, 137 (2005)
7. Ott, E., Antonsen, T.M.: Low dimensional behavior of large systems of globally coupled oscillators. Chaos **18**, 037113 (2008)
8. Omel'chenko, O.E., Wolfrum, M., Laing, C.R.: Partially coherent twisted states in arrays of coupled phase oscillators. Chaos **24**, 023102 (2014)
9. Hu, X., Boccaletti, S., Huang, W., Zhang, X., Liu, Z., Guan, S., Lai, C.-H.: Exact solution for first-order synchronization transition in a generalized Kuramoto model. Sci. Rep. **4**, 7262 (2014)
10. Wiley, D.A., Strogatz, S.H.: The size of the sync basin. Chaos **16**, 015103 (2006)
11. Hemmen, J.L., Wreszinski, W.F.: Lyapunov function for the kuramoto model of nonlinearly coupled oscillators. J. Stat. Phys. **72**, 145 (1993)
12. Tilles, P.F.C., Ferreira, F.F., Cerdeira, H.A.: Multistable behavior above synchronization in a locally coupled Kuramoto model. Phys. Rev. E **83**, 066206 (2011)
13. Girnyk, T., Hasler, M., Maistrenko, Y.: Multistability of twisted states in non-locally coupled kuramoto-type models. Chaos **22**, 013114 (2012)
14. Niu, B.: Codimension-two bifurcations induce hysteresis behavior and multistabilities in delay-coupled kuramoto oscillators. Nonlinear Dyn. **87**, 803 (2017)
15. Delabays, R., Tyloo, M., Jacquod, P.: The size of the sync basin revisited. Chaos **27**, 103109 (2017)
16. Ha, S.-Y., Kang, M.-J.: On the basin of attractors for the unidirectionally coupled Kuramoto model in a ring. SIAM J. Appl. Math. **72**, 1549 (2012)
17. Hong, H., Strogatz, S.H.: Kuramoto model of coupled oscillators with positive and negative coupling parameters: an

example of conformist and contrarian oscillators. Phys. Rev. Lett. **106**, 054102 (2011)

18. Cohen, A.H., Ermentrout, G.B., Kiemel, T., Kopell, N., Sigvardte, K.A., Williams, T.L.: Modelling of intersegmental coordination in the lamprey central pattern generator for locomotion. Trends Neurosci. **15**, 434 (1992)

19. Ermentrout, G.B., Kopell, N.: Inhibition-produced patterning in chains of coupled nonlinear oscillators. SIAM J. Appl. Math. **54**, 478 (1994)

20. Tsodyks, M., Kenet, T., Grinvald, A., Arieli, A.: Linking spontaneous activity of single cortical neurons and the underlying functional architecture. Science **286**, 1943 (1999)

21. Newman, J.P., Butera, R.J.: Mechanism, dynamics, and biological existence of multistability in a large class of bursting neurons. Chaos **20**, 023118 (2010)

22. Bronski, J.C., DeVille, L., Park, M.J.: Fully synchronous solutions and the synchronization phase transition for the finite-N Kuramoto model. Chaos **22**, 033133 (2012)

23. Wang, C., Rubido, N., Grebogi, C., Baptista, M.S.: Approximate solution for frequency synchronization in a finite-size kuramoto model. Phys. Rev. E **92**, 062808 (2015)

24. Sakaguchi, H., Kuramoto, Y.: A soluble active rotator model showing phase transitions via mutual entrainment. Prog. Theor. Phys. **76**, 576 (1986)

25. Burylko, O., Mielke, A., Wolfrum, M., Yanchuk, S.: Coexistence of hamiltonian-like and dissipative dynamics in chains of coupled phase oscillators with skew-symmetric coupling. SIAM J. Appl. Dyn. Syst. **17**, 2076 (2018)

26. Matheny, M.H., Emenheiser, J., Fon, W., Chapman, A., Salova, A., Rohden, M., Li, J., de Badyn, M.H., Pósfai, M., Duenas-Osorio, L., et al.: Exotic states in a simple network of nanoelectromechanical oscillators. Science **363**, eaav7932 (2019)

27. Yeldesbay, A., Pikovsky, A., Rosenblum, M.: Chimeralike states in an ensemble of globally coupled oscillators. Phys. Rev. Lett. **112**, 144103 (2014)

28. Abrams, D.M., Strogatz, S.H.: Chimera states for coupled oscillators. Phys. Rev. Lett. **93**, 174102 (2004)

29. Pikovsky, A., Rosenblum, M.: Partially integrable dynamics of hierarchical populations of coupled oscillators. Phys. Rev. Lett. **101**, 264103 (2008)

30. Motter, A.E.: Nonlinear dynamics: spontaneous synchrony breaking. Nat. Phys. **6**, 164 (2010)

31. Kuramoto, Y., Battogtokh, D.: Coexistence of coherence and incoherence in nonlocally coupled phase oscillators. Nonlinear Phenom. Complex Syst. **5**, 380 (2002)

32. Davis, P.J.: Circulant Matrices. Wiley, New York (1979)

33. Gopal, R., Chandrasekar, V.K., Venkatesan, A., Lakshmanan, M.: Observation and characterization of chimera states in coupled dynamical systems with nonlocal coupling. Phys. Rev. E **89**, 052914 (2014)

34. Zakharova, A., Kapeller, M., Schoöll, E.: Chimera death: symmetry breaking in dynamical networks. Phys. Rev. Lett. **112**, 154101 (2014)

35. Rakshit, S., Bera, B.K., Perc, M., Ghosh, D.: Basin stability for chimera states. Sci. Rep. **7**, 2412 (2017)

36. Wolfrum, M., Omel'chenko, O.E.: Chimera states are chaotic transient. Phys. Rev. E **84**, 015201(R) (2011)

37. Medeiros, E.S., Medrano-T, R.O., Caldas, I.L., Feudel, U.: Boundaries of synchronization in oscillator networks. Phys. Rev. E **98**, 030201(R) (2018)

38. Mihara, A., Medrano-T, R. O. et al., In preparation